Atomic Layer Deposition of SrS and BaS Thin Films Using Cyclopentadienyl Precursors

J. Ihanus,*,† T. Hänninen,† T. Hatanpää,† T. Aaltonen,† I. Mutikainen,† T. Sajavaara,‡ J. Keinonen,‡ M. Ritala,† and M. Leskelä†

Laboratory of Inorganic Chemistry, Department of Chemistry, P. O. Box 55, FIN-00014, University of Helsinki, Finland, and Accelerator Laboratory, Department of Physical Sciences, P. O. Box 43, FIN-00014, University of Helsinki, Finland

Received May 7, 2001. Revised Manuscript Received November 14, 2001

SrS and BaS thin films were grown on glass substrates using an atomic layer deposition (ALD) technique and $(C_5{}^iPr_3H_2)_2Sr(THF)$ (**1**), $(C_5Me_5)_2Sr(THF)_x$ (**2**), $(C_5Me_5)_2Ba(THF)_x$ (**3**), and H_2S as precursors. Deposition temperatures were 120−460, 155−400, and 180−400 °C with **1**, **2**, and **3**, respectively. Growth rate of the films varied between 0.6 and 3.0 Å/cycle and all the films were polycrystalline as deposited. The amount of C, H, and O residues was found to be 0.1−0.6 at. % in the films grown at 300 °C as determined by time-of-flight elastic recoil detection analysis (TOF-ERDA). Growth mechanisms for the films grown at different temperatures were also proposed. Crystal structures of **2** and **3** were determined.

Introduction

Alkaline earth metal sulfide thin films have received a lot of attention in recent years as host materials for luminescent layers in thin film electroluminescent devices, and particularly SrS:Ce and SrS:Cu are considered as blue-emitting phosphors.[1,2] These films can be prepared by different methods such as chemical vapor deposition (CVD),[3] electron beam evaporation (EBE),[4] molecular beam epitaxy (MBE),[5] multisource deposition,[6] reactive evaporation,[7] sputtering,[8] and atomic layer deposition (ALD),[9,10] which is also known as atomic layer epitaxy (ALE).[11−13] ALD is a special modification of CVD, based on alternately pulsed precursors that react on the substrates through self-limiting surface reactions. Both ALD and CVD methods need stable and volatile precursors and in practice the choice of alkaline earth metal precursors has been limited to β-diketonates and their adduct derivatives.[14] A problem of alkaline earth metal β-diketonates is, however, that they can oligomerize or react with impurities to compensate for the coordination unsaturation of the metal, which further on can change the precursor properties, like volatility. Alkaline earth metal cyclopentadienyl compounds can also be used as precursors in ALD and CVD, but so far only certain oxide materials have been deposited by ALD.[15,16] In this work $(C_5{}^iPr_3H_2)_2Sr(THF)$ (**1**), $(C_5Me_5)_2Sr(THF)_x$ (**2**), and $(C_5Me_5)_2Ba(THF)_x$ (**3**) have been used as Sr and Ba precursors to grow SrS and BaS thin films by ALD.

Experimental Section

Reagents and Methods for Synthesis of Precursors. Operations involving air-sensitive materials were carried out under argon using the standard Schlenk techniques and glovebox. Toluene and hexane were dried and stored over 4-Å molecular sieves. Tetrahydrofuran (THF) was freshly distilled from sodium benzophenone ketyl. Adogen 464 (Aldrich), anhydrous strontium iodide (Aldrich, 99.99+%), anhydrous barium iodide (Strem Chemicals, 97%), and 2-bromopropane (Acros, 99%) were used as-received. Potassium hydride (Merck) as a 35 wt % dispersion in mineral oil was washed with hexane and dried before use. Cyclopentadiene was prepared by thermal cracking of dicyclopentadiene (Pfaltz & Bauer, 95%). 1,2,3,4,5-Pentamethylcyclopentadiene (C_5Me_5H) was prepared according to the published procedure[17] and stored over 4-Å molecular sieves.

Characterization of Reagents and Precursors. ^1H and ^{13}C NMR spectra were recorded with a Varian Gemini 2000

* To whom correspondence should be addressed.
† Department of Chemistry.
‡ Department of Physical Sciences.

(1) Leskelä, M.; Li, W.-M.; Ritala, M. *Semiconductors and Semimetals, Electroluminescence II Vol 65*; Müller, G., Ed.; Academic Press: New York, 2000; p 107, and references therein.
(2) Rack, P. D.; Holloway, P. H. *Mater. Sci. Eng. R* **1998**, *21*, 171, and references therein.
(3) Barth, K. W.; Lau, J. E.; Peterson, G. G.; Endisch, D.; Kaloyeros, A. E.; Tuenge, R. T.; King, C. N. *J. Electrochem. Soc.* **2000**, *147*, 2174.
(4) Poelman, D.; Wauters, D.; Van Meirhaeghe, R. L.; Cardon, F. *Thin Solid Films* **1999**, *350*, 67.
(5) Xin, Y. B.; Tong, W.; Park, W.; Chaichimansour, M.; Summers, C. J. *J. Appl. Phys.* **1999**, *85*, 3999.
(6) Nakanishi, Y.; Ito, T.; Hatanaka, Y.; Shimaoka, G. *Appl. Surf. Sci.* **1993**, *65/66*, 515.
(7) Mauch, R. H.; Velthaus, K. O.; Bilger, G.; Schock, H. W. *J. Cryst. Growth* **1992**, *117*, 964.
(8) Morishita, T.; Matsuyama, H.; Matsui, M.; Tonomura, S.; Wakihara, M. *Appl. Surf. Sci.* **2000**, *157*, 61.
(9) Tammenmaa, M.; Antson, H.; Asplund, M.; Hiltunen, L.; Leskelä, M.; Niinistö, L.; Ristolainen, E. *J. Cryst. Growth* **1987**, *84*, 151.
(10) Saanila, V.; Ihanus, J.; Ritala, M.; Leskelä, M. *Chem. Vap. Deposition* **1998**, *4*, 227.
(11) Suntola, T. *Handbook of Crystal Growth 3*; Hurle, D. T. J., Ed.; Elsevier: New York, 1994; p 601.
(12) Ritala, M.; Leskelä, M. *Handbook of Thin Film Materials Vol 1*; Nalwa, H. S., Ed.; Academic Press: New York, 2002; p 103.
(13) Niinistö, L.; Ritala, M.; Leskelä, M. *Mater. Sci. Eng.* **1996**, *B41*, 23.
(14) Tiitta, M.; Niinistö, L. *Chem. Vap. Deposition* **1997**, *3*, 167.
(15) Huang, R.; Kitai, A. H. *J. Electron. Mater.* **1993**, *22*, 215.
(16) Vehkamäki, M.; Hatanpää, T.; Hänninen, T.; Ritala, M.; Leskelä, M. *Electrochem. Solid-State Lett.* **1999**, *2*, 504.
(17) Threlkel, R. S.; Bercaw, J. E.; Seidler, P. F.; Stryker, F. M.; Bergman, R. G. *Org. Synth.* **1987**, *65*, 42.

10.1021/cm0111130 CCC: $22.00
Published on Web 04/30/2002

instrument at ambient temperature. The type of carbon and hydrogen atoms was determined via DEPT and $^{13}C-^{1}H$ and $^{1}H-^{1}H$ COSY techniques. Chemical shifts were referenced to $SiMe_4$ and are given in ppm. Thermal analyses were carried out on a Mettler Toledo TA8000 system equipped with a TGA850 thermobalance using a flowing nitrogen atmosphere at 1 atm. The heating rate in thermogravimetry (TG) was 10 °C/min and weights of the samples were between 16 and 18 mg.

Preparation of $C_5{}^{i}Pr_3H_3$. KOH (842 g, 15 mol) was dissolved in water (842 g, 47 mol) and the solution was poured into a three-neck round-bottom flask fitted with a condenser, mechanical stirrer, oil bath, and thermometer. Adogen 464 (20 g), cyclopentadiene (33 g, 0.5 mol), and 2-bromopropane (246 g, 2.0 mol) were added and the reaction was carried out as reported in the literature.[18] Amounts of byproducts were decreased by using 4 equiv of isopropyl bromide, instead of 5, in proportion to cyclopentadiene. After chromatography and evaporation of the solvent, the crude product was combined with another batch prepared similarly and vacuum-distilled using a 300-mm Vigreux column. The fraction boiling at 67−70 °C at 6 Torr produced 157 g (82%) of yellow oily liquid, which was predominantly 1,2,4-triisopropylcyclopenta-1,3-diene, but contained also small quantities of other substitution products. For pure 1,2,4-triisopropylcyclopenta-1,3-diene (obtained by hydrolyzing $K(C_5{}^{i}Pr_3H_2)$) ^{1}H NMR (C_6D_6) 1.06, 1.10, 1.12 (3d, $^{3}J = 6.83$ Hz, 18H, C*H*$_3$), 2.57 (septet of doublets, $^{3}J = 6.83$ Hz, $^{4}J = 1.50$ Hz, 1H, C*H*Me$_2$), 2.77 (s, 2H, C*H*$_2$), 2.83, 2.88 (2 septets, $^{3}J = 6.83$ Hz, 2H, C*H*Me$_2$), 6.18 (d, $^{4}J = 1.20$ Hz, 1H, ring-C*H*); $^{13}C\{^{1}H\}$ NMR (C_6D_6) 22.94 (*C*H$_3$), 23.20 (*C*H$_3$), 23.96 (*C*H$_3$), 26.33 (*C*HMe$_2$), 27.08 (*C*HMe$_2$), 30.18 (*C*HMe$_2$), 39.16 (ring-*C*H$_2$), 124.03 (ring-*C*H), 141.59, 143.91, 152.31 (ring-*C*'*s*).

Preparation of $K(C_5{}^{i}Pr_3H_2)$. In a typical preparation $C_5{}^{i}Pr_3H_3$ (28.0 g) was added dropwise to a stirred suspension of KH (5.4 g, 0.14 mol) in THF (200 mL) and reaction was carried out as described by Williams et al.[18] After refluxing, the clear dark brown solution was stirred for 3 h at room temperature whereupon the product began to crystallize. The mixture was then allowed to stand without stirring overnight and finally at −20 °C for 2 days. The resulting crystalline $K(C_5{}^{i}Pr_3H_2)$ was filtered, washed with hexane several times, and dried under vacuum. The product can be stored under argon at ambient temperature over 1 year. Yield: 22.0 g (66%). ^{1}H NMR (DMSO-d_6) 1.05, 1.06 (2d, $^{3}J = 6.75$ Hz, 18H, C*H*$_3$), 2.66 (septet, $^{3}J = 6.75$ Hz, 1H, C*H*Me$_2$), 2.76 (septet, $^{3}J = 6.75$ Hz, 2H, C*H*Me$_2$), 5.01 (s, 2H, ring-C*H*); $^{13}C\{^{1}H\}$ NMR (DMSO-d_6) 25.64 (*C*H$_3$), 26.32 (*C*H), 26.51 (*C*H$_3$), 28.67 (*C*H), 94.73 (ring-*C*H), 120.13, 122.20 (ring-*C*'*s*).

Synthesis of $(C_5{}^{i}Pr_3H_2)_2Sr(THF)$ (1). The mixture of anhydrous SrI_2 (5.0 g, 14.6 mmol) and $K(C_5{}^{i}Pr_3H_2)$ (6.8 g, 29.5 mmol) in THF (250 mL) was stirred for 3 days at room temperature. The solvent was removed under reduced pressure and toluene (250 mL) was added to the residue. The suspension was stirred overnight and filtered through Kieselguhr and the resulting solution was evaporated to dryness under vacuum using an oil bath (50 °C). The product was allowed to stand in the slowly cooling bath under vacuum for ca. 4 h. No changes in NMR spectra and reactivity of the substituted cyclopentadiene were observed after 12-month storage at −20 °C. The yield in 23 equal syntheses varied from 6.1 to 7.4 g (77−94%). The average was 6.9 g (87%), mode 7.0 g (88%), and standard deviation 0.36 g (4.5%). ^{1}H NMR (C_6D_6) 1.26 (m, 4H, THF), 1.31, 1.32, 1.33 (3d, $^{3}J = 6.76$ Hz, 36H, C*H*$_3$), 2.94 (septet, $^{3}J = 6.76$ Hz, 2H, C*H*Me$_2$), 3.00 (septet, $^{3}J = 6.76$ Hz, 4H, C*H*Me$_2$), 3.42 (m, 4H, THF), 5.79 (s, 4H, ring-C*H*); $^{13}C\{^{1}H\}$ NMR (C_6D_6) 25.17 (THF), 25.31 (*C*H$_3$), 25.34 (*C*H$_3$), 26.46 (*C*H$_3$), 26.90 (*C*H), 29.22 (*C*H), 69.68 (THF), 101.71 (ring-*C*H), ca. 127.6 (ring-*C*, obscured by solvent peak), 129.31 (ring-*C*).

Preparation of $K(C_5Me_5)$. Pentamethylcyclopentadiene (15.0 g, 0.11 mol) was added in small portions via syringe to a stirred suspension of KH (4.4 g, 0.11 mol) in THF (250 mL). Evolution of hydrogen and formation of a white precipitate was observed. The mixture was then refluxed for 1 h and allowed to stand overnight at room temperature. The product was filtered, washed with THF (20 mL), and dried under reduced pressure for 12 h. Yield: 15.2 g (79%). ^{1}H NMR (DMSO-d_6) 1.84 (s, C*H*$_3$); $^{13}C\{^{1}H\}$ NMR (DMSO-d_6) 12.32 (*C*H$_3$), 103.70 (ring-*C*'*s*).

Synthesis of $(C_5Me_5)_2Sr(THF)_x$ (2). The procedure was as described for complex **1** with SrI_2 (4.1 g, 12 mmol), $K(C_5Me_5)$ (4.5 g, 26 mmol), THF (150 mL), and toluene (ca. 150 mL). The temperature of the oil bath was 90 °C and the residue was allowed to stand in the slowly cooling bath for ca. 2 h after evaporation of the solvent. The THF content of powdery product varied from batch to batch; see results. Yield for $x = 1.2$: 4.6 g (87%). ^{1}H NMR (C_6D_6) 1.23 (m, THF), 2.08 (s, 30H, C*H*$_3$), 3.14 (m, THF); $^{13}C\{^{1}H\}$ NMR (C_6D_6) 11.03 (*C*H$_3$), 25.28 (THF), 68.47 (THF), 112.26 (ring-*C*'*s*).

Synthesis of $(C_5Me_5)_2Ba(THF)_x$ (3). Pentamethylcyclopentadiene (5.7 g, 42 mmol) dissolved in THF (100 mL) was added in small portions via a pressure-equalized dropping funnel to a stirred suspension of KH (1.7 g, 42 mmol) in THF (100 mL). Evolution of hydrogen and formation of a white precipitate was observed. The mixture was stirred overnight at room temperature. Anhydrous BaI_2 (8.2 g, 21 mmol) was added and the solution was stirred for 2 days at room temperature. The solvent was removed under reduced pressure and toluene (250 mL) was added to the residue. The suspension was stirred overnight and filtered through Kieselguhr, and the resulting solution was evaporated to dryness under vacuum using a water bath (40 °C). The light yellow product was allowed to stand in the slowly cooling bath under vacuum for ca. 4 h, crushed, and packed into glass vials. The average yield for $x = 1.25$: 5.1 g (48%). ^{1}H NMR (C_6D_6) 1.30 (m, THF), 2.13 (s, 30H, C*H*$_3$), 3.29 (m, THF); $^{13}C\{^{1}H\}$ NMR (C_6D_6) 11.23 (*C*H$_3$), 25.36 (THF), 68.04 (THF), 112.83 (ring-*C*'*s*).

Single-Crystal X-ray Structure Determination. The summary of the crystal data, intensity collection, and refinement is given in the Supporting Information. Unit-cell parameters for both structures were determined using 25 well-centered reflections measured with a Rigaku AFC-7S diffractometer. Data collections were made at 193 K with crystals fixed at fibers using the oil-drop technique.[19] Data were reduced by the TEXSAN program package.[20] Structures were solved using direct methods, SIR-92,[21] and refined using the SHELXL-97 program package.[22] Illustrations were produced by the SHELXTL PLUS program package.[23] Complex **2**: $C_{28}H_{46}O_2Sr$, fw = 502.27, 0.35 × 0.35 × 0.27 mm, $T = 193$ K, monoclinic, space group *C*2/*c* (No. 15), $a = 21.931(4)$ Å, $b = 20.688(4)$ Å, $c = 15.877(3)$ Å, $V = 5505(2)$ Å^3, $Z = 8$, $d_{calc} = 1.212$ g/cm^3, $\mu = 1.979$ mm^{-1}, $R_1 = 0.0686$, and $wR_2 = 0.1584$. Complex **3**: $C_{28}H_{46}O_2Ba$, fw = 551.99, 0.50 × 0.50 × 0.40 mm, $T = 193$ K, monoclinic, space group *C*2/*c* (No. 15), $a = 22.054(4)$ Å, $b = 20.556(4)$ Å, $c = 16.087(3)$ Å, $V = 5631(2)$ Å^3, $Z = 8$, $d_{calc} = 1.302$ g/cm^3, $\mu = 1.430$ mm^{-1}, $R_1 = 0.0409$, and $wR_2 = 0.1042$.

ALD Film Growth Experiments. The film growth experiments were carried out using a commercial hot-wall flow-type F-120 reactor (ASM Microchemistry Ltd., Finland) operating under a nitrogen pressure of ca. 10 mbar. The films were deposited by pulsing complexes **1**, **2**, or **3** and H_2S (Messer Griesheim 99.999%) alternately on Al_2O_3-covered 5 × 5 cm^2 glass substrates. N_2 (99.999%) was used as a carrier and purging gas with the flow rate of 400 sccm. **1**, **2**, and **3** were

(18) Williams, R. A.; Tesh, K. F.; Hanusa, T. P. *J. Am. Chem. Soc.* **1991**, *113*, 4843.

(19) Kottke, T.; Stalke, D. *J. Appl. Crystallogr.* **1993**, *26*, 615.

(20) *TEXSAN: Single-Crystal Structure Analysis Software*; Molecular Structure Corporation: The Woodlands, TX, 1993.

(21) Altomare, A.; Cascarano, G.; Giacovazzo, C.; Guagliardi, A. *J. Appl. Crystallogr.* **1993**, *26*, 343.

(22) Sheldrick, G. M. *SHELXL-97, Program for the Refinement of Crystal Structures*; University of Göttingen: Göttingen, Germany, 1997.

(23) Sheldrick, G. M. *SHELXTL-Plus, Release 5.03*; Siemens Analytical X-ray Instruments Inc.: Madison, WI, 1994.

evaporated from open quartz boats inside the reactor and they were pulsed on the substrates by means of inert gas valving.[11] The evaporation temperatures in the standard experiments were 100, 140, and 160 °C for **1**, **2**, and **3**, respectively. Since the complexes are air-sensitive, they were loaded inside an Ar-filled glovebox to the boats that were put further into closed glass tubes. The air exposure was minimized by taking the boats out from the glass tubes just before they were inserted into the reactor. H_2S was pulsed into the reactor using a solenoid valve and the flow rate was adjusted to 5 sccm during a continuous flow with the aid of a needle valve and a mass flowmeter. Samples for the time-of-flight elastic recoil detection analysis (TOF-ERDA) and atomic force microscopy (AFM) analysis were covered with a thin Al_2O_3 layer by ALD in the same pump down after the SrS and BaS deposition. Source chemicals for the Al_2O_3 were trimethylaluminum (TMA) and H_2O, which were pulsed alternately using needle and solenoid valves. Both TMA and H_2O were kept outside the reactor at room temperature. Pulse and purge lengths for TMA and H_2O were 0.4 and 0.5 s, respectively. Growth temperatures for Al_2O_3 were the same as those for SrS and BaS and thicknesses of the Al_2O_3 layers were evaluated to be 25−60 nm depending on the sample.

Characterization of Films. Film thicknesses and refractive indices were evaluated by fitting transmittance spectra using a procedure developed by Ylilammi and Ranta-aho.[24] The spectra were measured in the wavelength region of 370−1100 nm (Hitachi U-2000) and the refractive index was evaluated at 580 nm. Film crystallinity was examined with a powder X-ray diffractometer using Cu Kα radiation (Philips MPD 1880). Atomic force microscopy (AFM) measurements were carried out in air in contact mode (Thermomicroscopes Auto-Probe CP Research AFM). Root-mean-square (RMS) roughness values were determined from the AFM images using the software of the microscope. The elemental depth profiles of the films were determined with a TOF-ERDA using a beam of 34 MeV $^{127}I^{6+}$ or 53 MeV $^{127}I^{10+}$ ions obtained from an EGP-10-II tandem accelerator.[25] The recoiled atoms were detected at an angle of 40° and the sample was tilted 20° relative to the beam direction. In TOF-ERDA both the velocity and energy of the recoils are measured and therefore different masses can be separated and elemental energy spectra obtained. These energy spectra are converted to depth profiles on the basis of the measurement geometry, elastic scattering cross sections, and stopping powers. The reported elemental contents were always integrated from the middle of the sulfide films to minimize the influence of the oxide layers above and below.

Results

Precursor Syntheses. Precursor syntheses mainly followed published procedures,[18,26,27] but modifications and additional details are given in this paper. Full lists of ^1H and ^{13}C NMR chemical shifts are provided in the Experimental Section because the earlier published data are not complete.

In the synthesis of $(C_5{}^iPr_3H_2)_2Sr(THF)$ a monosolvated product was obtained in all 23 batches as shown by ^1H NMR spectra. In contrast to the earlier report,[26] all three expected resonances for the methyl carbons were observed in ^{13}C NMR spectra, although the difference between two of them was small, only 0.03 ppm. In the case of $(C_5Me_5)_2Sr(THF)_x$ the degree of THF solvation was different for each of the four batches prepared, x ranging from 1.2 to 1.6. On the other hand, crystallization from THF gave the disolvated product as shown by X-ray crystallography. Similar results ($x = 1.2-1.6$) were obtained for $(C_5Me_5)_2Ba(THF)_x$. Clearly, the evaporation of toluene (at 90 °C for **2** and 40 °C for **3**) caused partial loss of the second THF. This kind of a procedure for removal of the coordinated Lewis base from metallocene is known as a toluene reflux method in the literature.[28]

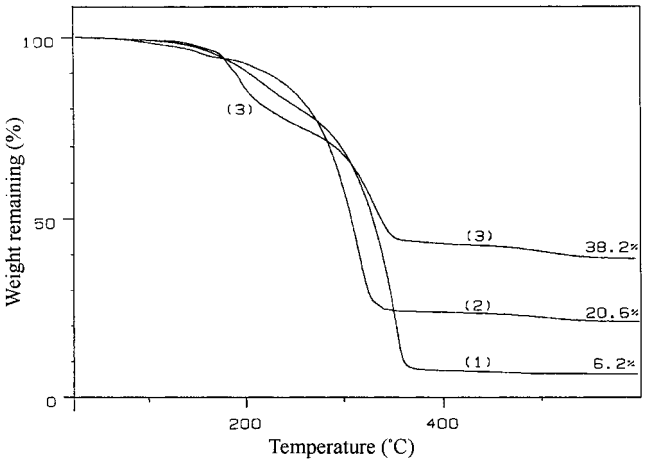

Figure 1. TG curves of $(C_5{}^iPr_3H_2)_2Sr(THF)$ (**1**), $(C_5Me_5)_2Sr(THF)_{1.2}$ (**2**), and $(C_5Me_5)_2Ba(THF)_2$ (**3**).

Cream-colored $(C_5{}^iPr_3H_2)_2Sr(THF)$ was less sensitive to air than $(C_5Me_5)_2Sr(THF)_x$ or $(C_5Me_5)_2Ba(THF)_x$ but turned yellow and orange after short exposure to air. $(C_5Me_5)_2Sr(THF)_x$ was obtained as an off-white solid, which decomposed and changed its color to yellow and brown when contacted with air. $(C_5Me_5)_2Ba(THF)_x$ was light yellow and turned to brown when contacted with air. Obviously, the larger $(C_5{}^iPr_3H_2)^-$ ligands give better protection for the metal than $(C_5Me_5)^-$. All the complexes could be stored over 1 year in a dark place under argon at room temperature without observable decomposition.

Thermal Analyses of the Precursors. TG curves for the complexes are presented in Figure 1. $(C_5{}^iPr_3H_2)_2Sr(THF)$ and $(C_5Me_5)_2Sr(THF)_{1.2}$ leave residues of 6.2 and 20.6% while $(C_5Me_5)_2Ba(THF)_2$ leaves a residue of 38.2%. In the TG curves of $(C_5Me_5)_2Sr(THF)_{1.2}$ and $(C_5{}^iPr_3H_2)_2Sr(THF)$ it is not possible to distinguish different steps while from the DTG curve of $(C_5Me_5)_2Ba(THF)_2$ (not shown) three steps could be seen. The first one (−25.8%) at 105−260 °C is assigned to release of the two THF molecules (theoretically −26.1%), the second at 260−415 °C to evaporation of $(C_5Me_5)_2Ba$ and possible decomposition products (−32.0%), and the last at 415−600 °C to evaporation of some decomposition products (−4.0%). Though distinct steps cannot be distinguished in the case of $(C_5{}^iPr_3H_2)_2Sr(THF)$ and $(C_5Me_5)_2Sr(THF)_{1.2}$ the same steps may be present but overlapping. The TG curve for $(C_5Me_5)_2Ba(THF)_{1.6}$ (not shown) is similar to the curve of $(C_5Me_5)_2Sr(THF)_{1.2}$ but the residue is larger, 45.3%. All the complexes studied seem to lose the coordinated THF before or simultaneously with evaporation of the unsolvated complex.

One obvious reason for the high amount of residues is the decomposition of the complexes during the TG

(24) Ylilammi, M.; Ranta-aho, T. *Thin Solid Films* **1993**, *232*, 56.
(25) Jokinen, J.; Keinonen, J.; Tikkanen, P.; Kuronen, A.; Ahlgren, T.; Nordlund, K. *Nucl. Instrum. Methods* **1996**, *119*, 533.
(26) Burkey, D. J.; Williams, R. A.; Hanusa, T. P. *Organometallics* **1993**, *12*, 1331.
(27) McCormick, M. J.; Williams, R. A.; Levine, L. J.; Hanusa, T. P. *Polyhedron* **1988**, *7*, 725.
(28) Wojtczak, W. A.; Fleig, P. F.; Hampden-Smith, M. J. *Adv. Organomet. Chem.* **1996**, *40*, 215, and references therein.

Table 1. Amount of C, H, and O in the SrS and BaS Thin Films Determined by TOF-ERDA

metal source and the growth temperature	C (at. %)	H (at. %)	O (at. %)
	$(C_5{}^iPr_3H_2)_2Sr(THF)$ (**1**)		
120 °C	1.0	2.6	0.6
200 °C	0.2	0.8	0.5
300 °C	0.1	0.5	0.6
400 °C	1.9	0.8	0.3
	$(C_5Me_5)_2Sr(THF)_x$ (**2**)		
200 °C	0.4	1.3	0.6
300 °C	0.1	0.3	0.3
	$(C_5Me_5)_2Ba(THF)_x$ (**3**)		
200 °C	0.1	0.8	0.3
300 °C	0.1	0.3	0.3

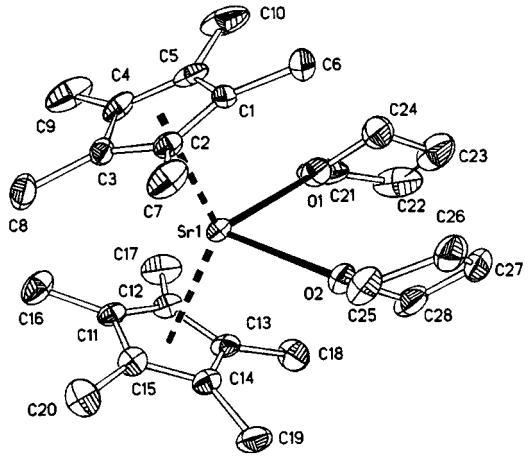

Figure 2. View of $(C_5Me_5)_2Sr(THF)_2$ (**2**) with atomic labeling. Ellipsoids are drawn on the 30% probability level. H atoms are omitted for clarity. Distances from the strontium to the ring centers are 2.602(7) and 2.604(7) Å. The angle (α) between geometrical centers of both rings and the strontium center is 135.2(2)° and the angle (β) between the ring normals and the strontium center is 136.8(2)°, confirming the very small "ring slippage".

analysis, which reflects the temperature instability of the complexes. A second possible reason for the residues is that the complexes make short contact with air before the TG analysis and may thus become oxidized into compounds that do not evaporate. Thickness profiles and darkness of the films deposited at ≥400 °C and carbon residue in the film deposited at 400 °C (cf. Table 1) indicate that complexes decompose because of high temperature and support the assumption that residues in the TG analysis are mainly due to thermal decomposition. Residues of the pentamethyl-substituted complexes in the TG analysis were clearly higher than those of the isopropyl-substituted, which indicates that the isopropyl ligand gives better protection against decomposition.

Single-Crystal X-ray Structures. A crystal structure determination summary is presented in the Supporting Information. Figures 2 and 3 show structures of **2** and **3**, respectively. The complexes crystallize as isomorphic monomers with a characteristically bent metallocene arrangement of the ligands around Sr and Ba. Both complexes can be considered as "simple bent" compounds on the basis that the planes of the cyclopentadienyl rings are nearly perpendicular to each other, 90.8(2)° in complex **2** and 89.6(2)° in complex **3**. The crystal structure of **1** was published earlier.[29]

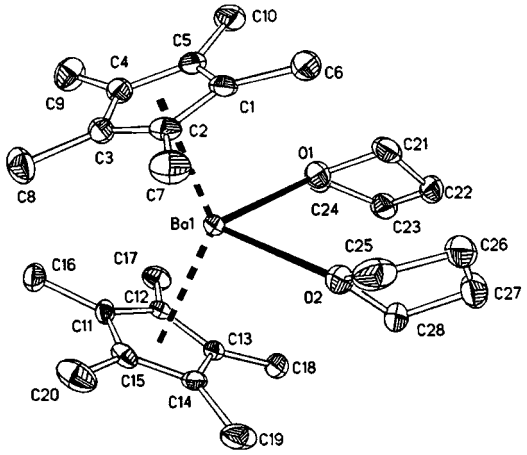

Figure 3. View of $(C_5Me_5)_2Ba(THF)_2$ (**3**) with atomic labeling. Ellipsoids are drawn on the 30% probability level. H atoms are omitted for clarity. Distances from the barium to ring centers are 2.751(5) and 2.764(5) Å. The angle between geometrical centers of both rings and the barium center is 137.4(2)° and the angle between ring normals and the barium center is 136.6(2)°.

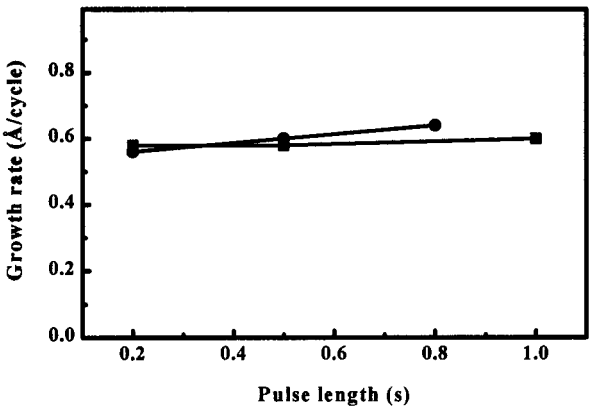

Figure 4. Growth rate of SrS as a function of the pulse length at the growth temperature of 380 °C. ● denotes the pulse length of $(C_5{}^iPr_3H_2)_2Sr(THF)$ (**1**) when the H_2S pulse length was 1.0 s. ■ denotes the H_2S pulse length when the pulse length of **1** was 0.5 s.

Growth of SrS Thin Films Using $(C_5{}^iPr_3H_2)_2Sr(THF)$ (1) as a Sr Source. In an ideal ALD process, parameters such as precursor evaporation temperature, pulse length, and purge length should not have an effect on the growth rate of the desired film material, provided that they exceed certain minimum values.[11] Figure 4 shows the growth rate of SrS at 380 °C as a function of the pulse lengths and Figure 5 as a function of the evaporation temperature of **1**. A very slight increase of the growth rate along with the pulse length of **1** can be seen, which is not surprising because **1** starts to decompose close to 400 °C as later will be shown in the characterization chapter. Doubling the pulse length at 200 °C did not increase the growth rate, which shows that the surface reactions are self-limiting also at growth temperatures below the constant growth rate region (see below). However, doubling the pulse length at 420 °C increased the growth rate ca. 40% because of the decomposition of complex **1**. Otherwise, it can be said that the growth rate is not dependent on either the pulse lengths or the evaporation temperature. Since a

(29) Burkey, D. J.; Hanusa, T. P. *Acta Crystallogr.* **1996**, *C52*, 2452.

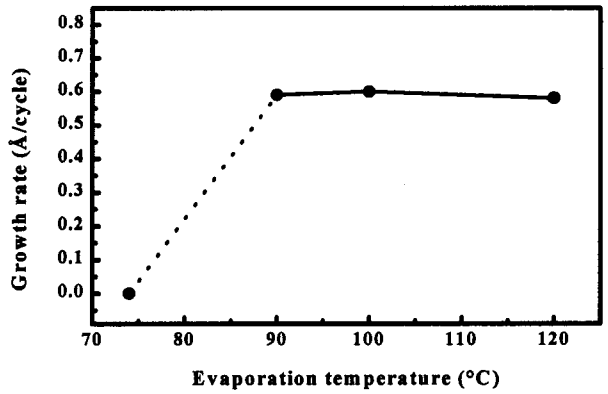

Figure 5. Growth rate of SrS as a function of the evaporation temperature of $(C_5{}^iPr_3H_2)_2Sr(THF)$ (**1**). The growth temperature was 380 °C.

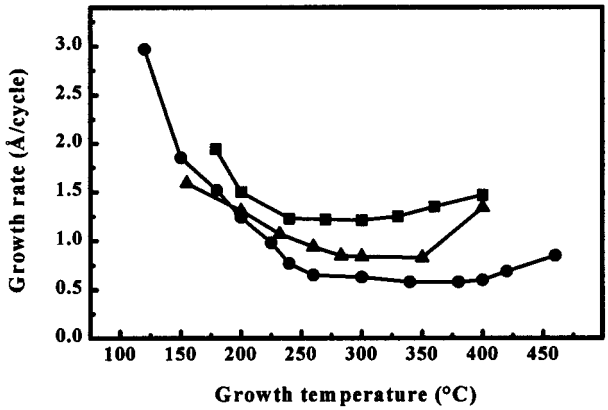

Figure 6. Growth rate of SrS and BaS as a function of the growth temperature. ●, ▲, and ■ denote $(C_5{}^iPr_3H_2)_2Sr(THF)$ (**1**), $(C_5Me_5)_2Sr(THF)_x$ (**2**), and $(C_5Me_5)_2Ba(THF)_x$ (**3**) as metal sources, respectively.

variation of the purging times between 0.2 and 1.0 s did not have an effect on the growth rate either, basic parameters for the rest of the experiments were selected to be 0.5-s pulse and purge lengths and 100 °C as an evaporation temperature.

The films were deposited at 120−460 °C and it can be seen that with **1** there is a wide temperature window between 260 and 400 °C where the growth rate is independent of the growth temperature (Figure 6). The growth rate varies between 0.6 and 3.0 Å/cycle, being lowest at the constant growth rate region. Deposition experiments at 300 °C showed that the growth rate was constant between 1500 and 15000 cycles, indicating that the thickness of the SrS films can be controlled simply just by adjusting the number of deposition cycles. All the above results show that SrS thin films can be deposited using **1** as a Sr source and the growth rate stays constant regardless of some process parameter variations, which is an inherent property of the ALD technique.

Growth of SrS Thin Films Using $(C_5Me_5)_2Sr(THF)_x$ (2) as a Sr source. Initially, the evaporation temperature of **2** and the pulse lengths were varied, and since the growth rate was unaffected, the rest of the experiments were done with 140 °C as the evaporation temperature and 0.5 s as the pulse lengths. Figure 6 shows the growth rate of SrS films as a function of the growth temperature. The films were deposited at 155−400 °C and it can be seen that the growth rate is constant between 280 and 350 °C. This is a much narrower temperature window than that with **1** as a Sr source. The growth rate varies between 0.8 and 1.6 Å/cycle, being again lowest at the constant growth rate area.

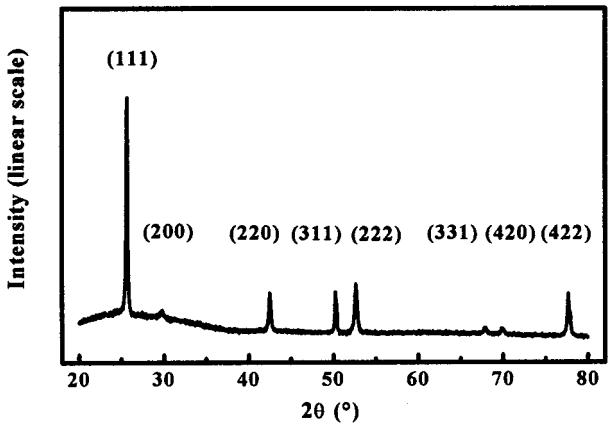

Figure 7. X-ray diffractogram of a SrS thin film deposited at 120 °C with complex **1** as a Sr source. The fwhm value of the (111) orientation is 0.20°.

Growth of BaS Thin Films Using $(C_5Me_5)_2Ba(THF)_x$ (3) as a Ba source. According to the initial experiments that showed no dependence of the growth rate on the evaporation temperature of **3** and pulse lengths, 160 °C was chosen as an evaporation temperature and 0.5 s as pulse lengths for the rest of the experiments. The BaS films were deposited at 180−400 °C and Figure 6 shows that the constant growth rate range is between 240 and 300 °C. The growth rate varies between 1.2 and 1.9 Å/cycle, being lowest at the constant growth rate area.

Characterization of the Films. Refractive indices of the SrS films were 2.0−2.1, being in accordance with the literature value[30] of 2.107. Refractive indices of the BaS films were around 2.1, being also in accordance with the literature value[31] of 2.155. All the films deposited in the course of this work were polycrystalline as deposited and thickness variations over the substrates were negligible up to the growth temperatures where the constant growth rate region ends (cf. Figure 6). Figure 7 shows as an example a diffractogram of the SrS film deposited at 120 °C using complex **1** as a Sr source. Even at this low temperature the film had good crystallinity as indicated by the high intensity and narrow peak widths. The XRD also showed some preferential (111) orientation in all films regardless of growth temperature.

Figures 8 and 9 show AFM images of SrS and BaS thin films. All the samples for the analysis were covered with a thin Al_2O_3 layer to protect them from a reaction with air. SrS films grown in the constant growth rate region are quite smooth, but the film grown at 120 °C has large grains, resulting also in higher roughness values than the other SrS films. On the other hand, the BaS film is quite similar to the SrS film grown at 120 °C, even though the BaS film was deposited in the constant growth rate region. Possible reason for rough-

(30) *CRC Handbook of Chemistry and Physics*, 54th ed; CRC Press: Cleveland, OH, 1973−74; p B-143.
(31) *CRC Handbook of Chemistry and Physics*, 54th ed; CRC Press: Cleveland, OH, 1973−74; p B-71.

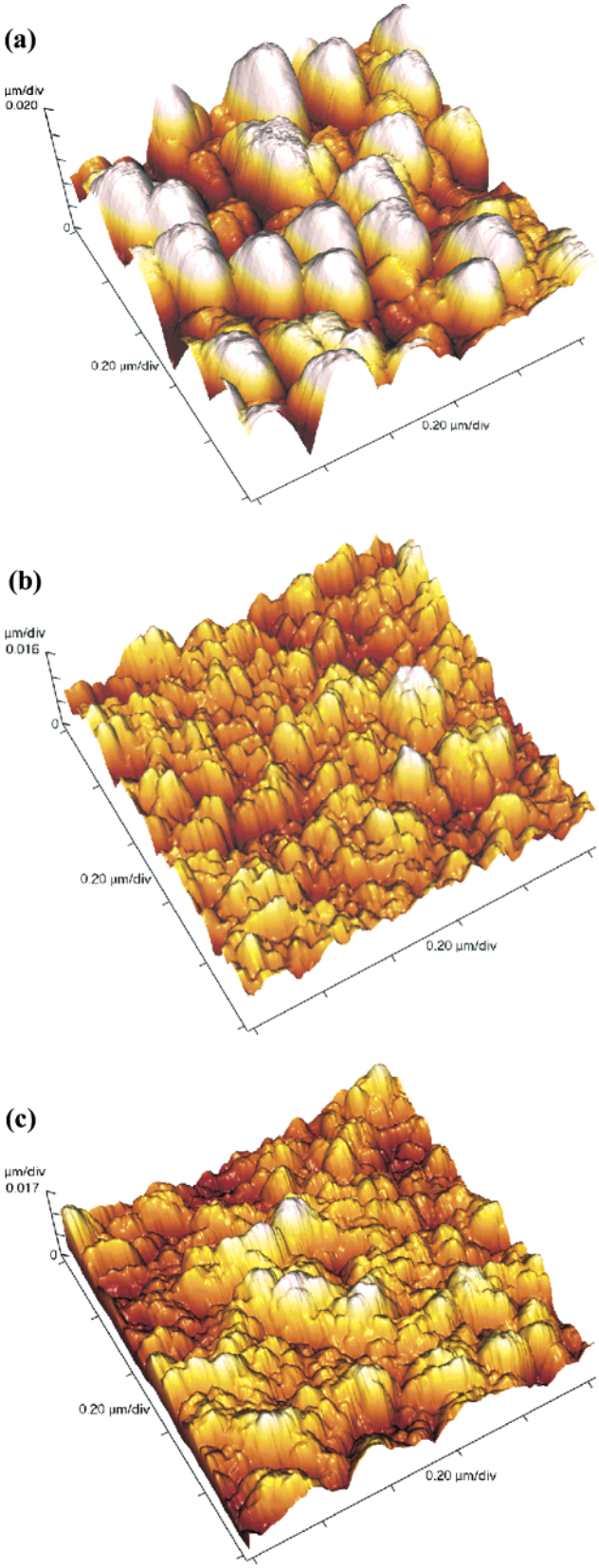

Figure 8. AFM images of SrS thin films grown at different temperatures when complex **1** was used as a Sr source. Growth temperatures (T), RMS values, and thicknesses (d) of the films are as follows: (a) $T = 120$ °C, RMS = 15 nm, $d = 480$ nm; (b) $T = 300$ °C, RMS = 6 nm, $d = 510$ nm; (c) $T = 400$ °C, RMS = 7 nm, $d = 420$ nm. The RMS values were determined from 4×4 μm images.

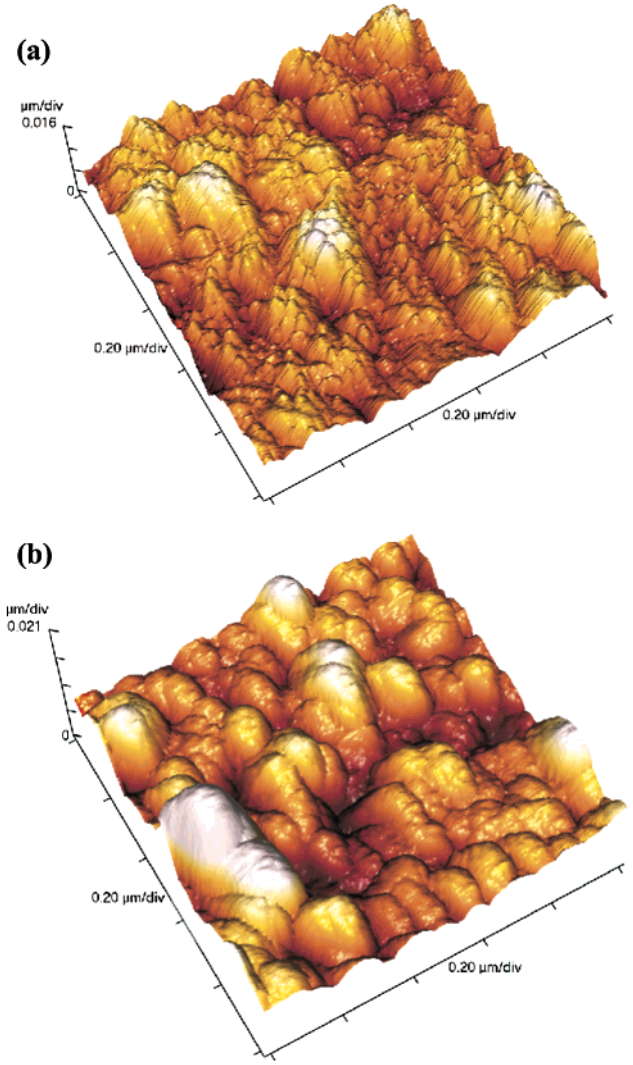

Figure 9. AFM images of SrS and BaS thin films grown at 300 °C when complexes **2** and **3** were used as Sr and Ba sources, respectively. RMS values and thicknesses (d) of the films are as follows: (a) SrS, RMS = 6 nm, $d = 540$ nm; (b) BaS, RMS = 11 nm, $d = 460$ nm. The RMS values were determined from 4×4 μm images.

ening can be that initial nucleation density in the rough samples is lower than in the flatter samples and thus the grains may grow for a longer time independently in three dimensions before coming into contact with each other. Such a relation between low nucleation density and formation of large grains and rough surface has been found earlier in ALD of polycrystalline ZnS on mica.[32] On the other hand, low mobility of the surface species may be one reason for the rough SrS film obtained at 120 °C because mobility of surface species is higher at higher temperatures, resulting in smoother films.

The amounts of the C, H, and O residues in the films grown at different temperatures were determined by TOF-ERDA (Table 1). All the samples for the analysis were covered with a thin Al_2O_3 layer since the unprotected samples reacted with air, resulting in remarkably higher amounts of impurities. On the other hand, the top protection layer can also be a source for the oxygen,

(32) Ihanus, J.; Ritala, M.; Leskelä, M.; Prohaska, T.; Resch, R.; Friedbacher, G.; Grasserbauer, M. *Appl. Surf. Sci.* **1997**, *120*, 43.

and it can cause interference signals in the TOF-ERDA measurements, resulting in an increase of the oxygen content in the analysis.[33] Since the oxide layer under the sulfide film can also cause an increase to the oxygen content in the analysis, Table 1 shows the upper limits to the amount of oxygen. The films grown with **1** as a Sr source do not show a lot of variation in the oxygen content. The SrS film grown at 120 °C has quite high carbon and hydrogen contents. The probable reason for this is that there is not enough thermal energy to fully complete the reactions between the precursors on the surface and to desorb all the reaction byproducts from the surface. The films grown at 200 and 300 °C have moderate impurity contents and the SrS film grown at 400 °C has high carbon content most probably because of the decomposition of **1**. The films deposited at 400 °C were also dark, which is considered as an indication of a high amount of carbon in the films. Table 1 shows also the impurity contents of the SrS films grown at 200 and 300 °C with complex **2** as a Sr source. Again, the amounts of C, H, and O are low at 300 °C, but at 200 °C the contents of C and H have increased, being higher than those with **1** as a Sr source. However, at the temperature range where the growth rate was constant, the amounts of the impurities were low with both **1** and **2**. Table 1 shows also that the amounts of C, H, and O in the BaS films were low both at 200 and at 300 °C. Finally, it is reminded that among the films deposited at 200 °C the amounts of C and H were the highest when complex **2** was used as a metal source and with **2** that deposition temperature is also furthest away from the constant growth rate region, when compared to the other complexes.

Comparison to Other ALD Studies on SrS and BaS Films. SrS and BaS thin films have been deposited earlier by ALD using $[Sr(thd)_2]_x$ and $[Ba(thd)_2]_x$ as Sr and Ba sources, respectively.[9,10,33−35] The as-deposited films have been polycrystalline-like in this study. The lowest growth temperatures for SrS and BaS have been 300 and 275 °C, as compared with 120 and 180 °C in the current work, respectively. Deposition temperatures <275 °C have not been used earlier because $[Sr(thd)_2]_x$ and $[Ba(thd)_2]_x$ complexes have been heated to >200 °C to ensure their sufficient volatilization. Growth rates of the SrS films[34,35] and their impurity contents[33] have been roughly at the same level as that in this study, but growth rates of the BaS films have been lower[9,10] and amounts of carbon and oxygen substantially higher[10] than those in the current work. There are also indications that the use of $[Sr(thd)_2]_x$ results in a rougher SrS surface[35] than the use of Sr complexes **1** or **2**.

Discussion

The growth rate curves of SrS and BaS show similar shapes (Figure 6). First, the growth rate decreases as a function of the temperature, then it stays constant, and finally it increases. Decreasing of the growth rate with increasing temperature has been observed in ALD of oxides and attributed to a decreasing number of surface −OH groups with increasing temperature.[36,37] The existence of surface −SH groups as reaction intermediates has been revealed in the ALD growth of CdS when dimethylcadmium and H_2S were used as precursors.[38] Temperature-programmed desorption (TPD) studies of the −SH groups formed in reactions at room temperature showed that they recombine and desorb as H_2S along with increasing temperature, peaking at ≈200 °C, and leave the surface covered with only sulfur.[38] Auger electron spectroscopy (AES) measurements of CdS films deposited by one ALD cycle showed also that the sulfur signal was reduced when the deposition temperature was increased, which suggests that less −SH groups can be formed at higher temperatures.[39] Interaction of H_2S with polycrystalline ZnO has been studied using synchrotron-based X-ray photoelectron spectroscopy (XPS).[40] The measurements showed that along with increasing temperature −SH groups on the surface decompose into a mixture of −SH and −S and the surface consists of only −S as the temperature is further increased.[40]

In this study the growth rates stop decreasing at 260, 280, and 240 °C and remain constant until 400, 350, and 300 °C with complexes **1**, **2**, and **3**, respectively. The decreasing growth rate may be related to a decreasing number of −SH groups left on the surface after the H_2S pulse. Therefore, it may be that at growth temperatures higher than ≈240−280 °C −SH groups are not formed anymore or they recombine with each other, immediately leaving the surface covered with only sulfur after the H_2S pulse. In principle, it might be possible that metal complexes would behave in the same way as the −SH groups; that is, complexes would recombine and desorb from the growth surface to an extent depending on the growth temperature, and at temperatures higher than ≈240−280 °C there would not be no more ligands attached on metal atoms on the surface. However, in that case the growth should not be self-limiting anymore and thus it should be possible to increase the amount of deposited metal atoms, and thereby the growth rate, just by increasing precursor dose. Recent studies on the use of complex **1** as a Sr source in the deposition of SrO and $SrTiO_3$ have shown that complex **1** can decompose around 300 °C.[41,42] However, the decomposition of the precursor appeared to be surface reaction rather than gas-phase decomposition because the growth rate increased as a function of the pulse length and deposition temperature but not as a function of the evaporation temperature.[41,42] Contrary to that, it was established in this study that the growth rate of the films saturates to a low level (cf. Figure 6), and increasing pulse time or evaporation temperature of the precursor does not

(33) Li, W.-M.; Ritala, M.; Leskelä, M.; Lappalainen, R.; Jokinen, J.; Soininen, E.; Hüttl, B.; Nykänen, E.; Niinistö, L. *J. Appl. Phys.* **1998**, *84*, 1029.
(34) Soininen, P.; Nykänen, E.; Niinistö, L.; Leskelä, M. *Chem. Vap. Deposition* **1996**, *2*, 69.
(35) Soininen, P.; Niinistö, L.; Nykänen, E.; Leskelä, M. *Appl. Surf. Sci.* **1994**, *75*, 99.
(36) George, S. M.; Ott, A. W.; Klaus, J. W. *J. Phys. Chem.* **1996**, *100*, 13121.
(37) Matero, R.; Rahtu, A.; Ritala, M.; Leskelä, M.; Sajavaara, T. *Thin Solid Films* **2000**, *368*, 1.
(38) Han, M.; Luo, Y.; Moryl, J. E.; Osgood, R. M., Jr. *Surf. Sci.* **1999**, *425*, 259.
(39) Luo, Y.; Han, M.; Slater, D. A.; Osgood R. M., Jr. *J. Vac. Sci. Technol.* **2000**, *A 18*, 438.
(40) Rodriguez, J. A.; Jirsak, T.; Chaturvedi, S.; Hrbek, J. *Surf. Sci.* **1998**, *407*, 171.
(41) Vehkamäki, M.; Hänninen, T.; Ritala, M.; Leskelä, M.; Sajavaara, T.; Rauhala, E.; Keinonen, J. *Chem. Vap. Deposition* **2001**, *7*, 75.
(42) Rahtu, A.; Hänninen, T.; Ritala, M. *J. Phys. IV France* **2001**, *11*, Pr3-923.

increase the growth rate (cf. Figures 4 and 5). Therefore, ligands seem to remain attached to Ba and Sr atoms on the sulfide surface during the metal precursor pulses, which implies differences between reactions on oxide and sulfide surfaces.

At growth temperatures higher than ≈240−280 °C the growth rate is constant because the surface termination is not changing anymore as a function of the temperature, and the growth rate is at minimum because the possible recombination process of the −SH groups has involved desorption of sulfur. At temperatures higher than the constant growth rate region the growth rate starts to increase again. The most probable reason for that is the decomposition of the complexes since at 420 °C the growth rate of SrS increased ≈40% by doubling the pulse length of complex **1** and thickness nonuniformity across the substrate was developed. The carbon content in the SrS film grown at 400 °C was clearly higher than at lower growth temperatures, showing that decomposition of complex **1** included also decomposition of the ligands (cf. Table 1).

Figure 6 shows that the growth rate of SrS is higher with complex **2** as a Sr source than with complex **1**. A possible reason for this is that the pentamethyl-substituted cyclopentadienyl complex creates less steric hindrance on the growth surface than the tri-isopropyl-substituted complex. Figure 6 shows also that the growth rate of BaS in the constant growth rate region is almost twice the growth rate of SrS when the same ligand was used for the metals. This difference is so large that the larger ion size of Ba cannot explain it alone and other reasons, like different reactivity of the precursors, must be involved.

Conclusions

New kinds of cyclopentadienyl precursors for ALD of SrS and BaS thin films were used. Large triisopropyl-substituted cyclopentadienyl ligands made the Sr precursor thermally more stable and less sensitive to air than the pentamethyl-substituted ligands. A growth temperature region where the growth rate was constant was found with every precursor. That region can be taken as an ideal deposition region because the amounts of C, H, and O were low in the films and the growth rate was dependent neither on the deposition temperature nor on the precursor doses. It was also possible to deposit polycrystalline sulfide films even below 200 °C. This can be especially advantageous in making electroluminescent displays where the alkaline earth sulfides have to be doped and the precursor for the dopant may be an organometallic compound that decomposes at low temperatures. Low growth temperatures make it also possible to use flexible polymer substrates, if desired.

Acknowledgment. This work was supported in part by the Academy of Finland and TEKES—The National Technology Agency of Finland. Ph.D. Jorma Koskimies is thanked for helpful discussion on organic syntheses and NMR spectra.

Supporting Information Available: Crystal data and structure refinement, atomic coordinates, complete lists of bond lengths and angles, displacement parameters, and listing of observed and calculated structure factors (PDF). This material is available free of charge via the Internet at http://pubs.acs.org.

CM0111130